Characterization of Swarm and Mainshock-Aftershock Behavior in Puerto Rico

Wilnelly Ventura-Valentin (1), Michael R. Brudzinski (1)(*)

(1) Miami University, Department of Geology and Environmental Earth Science, Oxford, OH

(*) Corresponding Author Contact Information:

Miami University

Department of Geology and Environmental Earth Science

250 S. Patterson Ave

Oxford, OH 45056 USA

brudzimr@MiamiOH.edu

513-280-0660

Declaration of Competing Interests:

The authors acknowledge there are no conflicts of interest recorded.

Abstract

The recent Indios, Puerto Rico earthquake sequence has drawn attention as the increased seismicity rate in this area was unprecedented. The sequence began on December 28, 2019, caused a 6.4 magnitude earthquake on January 7, 2020, and remained active over a year later. This sequence fits the nominal definition of an earthquake swarm in that it had an abrupt onset, a sustained high rate of seismicity without a clear triggering mainshock or evidence for Omori decay, and a lack of adherence to Bath's Law. However, the sequence also had several prominent mainshock-aftershock (MS-AS) sequences embedded within it. We applied 3-station waveform cross-correlation to the early part of this sequence using the Puerto Rico Seismic Network (PRSN) catalog as templates, which confirmed the mixture of swarm and MS-AS patterns. In an effort to place this intriguing sequence in the context of the previous seismicity in Puerto Rico, we investigated the existence of swarms and MS-AS sequences recorded by the PRSN since 1987 by identifying sequences with increased seismicity rate when compared to the background rate. 59 sequences were manually verified and characterized into swarms or MS-AS. We found 58% of the sequences follow traditional swarm patterns and 14% adhere to traditional MS-AS behavior while 29% of the sequences have a mixture of both swarm and MS-AS behaviors. These findings suggest it is not unusual for the Indios sequence to have a mixture of both characteristics. In addition, the detection of many swarms distributed over a broad area of the subduction interface indicates stress heterogeneity and low coupling consistent with prior studies indicating that the potential for a magnitude ~8 megathrust earthquake along the Puerto Rico Trench is unlikely.

I. Introduction

Puerto Rico lies in a dynamic plate boundary zone in between the North American and the Caribbean tectonic plates (*Calais et al*., 1992). Eastern Hispaniola, Puerto Rico and the Virgin Islands are the remnants of an intra-oceanic arc that formed in between the North American and Caribbean Plate boundary in the Cretaceous-early Paleogene period (*Chaytor and ten Brink*, 2010; *Donnelly*, 1989). The Northern Caribbean Plate boundary zone is predominantly controlled by left-lateral motion, collision, and oblique subduction of the North American plate beneath the Caribbean plate (*Chaytor and ten Brink*, 2010). This has resulted in the establishment of three microplates: Gonave (*Mann et al*., 1995), Hispaniola (*Byrne et al*., 1985), and the Puerto Rico-Virgin Island (PRVI) (*Jansma et al*., 2000).

The PRVI microplate is bounded in the north by the deepest trench in the Atlantic (Puerto Rico Trench) along with a complicated subducting slab morphology, while the eastern edges are delimited by the 19N fault zone characterized by normal motion, the Virgin Island Basin, and the Anegada Passage (*Dillon et al.*, 1999; *ten Brink*, 2005; *Meighan et al.*, 2013). The southern edge is defined by the Muertos Trough convergence zone with a low seismicity rate, and the western edge is represented by the Mona Passage which has been described to be extensional (Figure 1) (*Huérfano et al.*, 2005; *Jansma et al.*, 2000; *Chaytor and ten Brink*, 2010; *Granja Bruña et al.*, 2015). Moving inland, the island is divided in three by the Great Northern and Southern Puerto Rico Fault Zones (Figure 1) (*Huérfano et al.*, 2005). Overall, this creates a seismically active region that generates hundreds of earthquakes per year, but with most of the seismic activity small enough to not be felt by humans (M<4). However, historical seismicity records show that the northern part of PRVI have only seen moderate sized (M5.0-M5.9) earthquakes when compared to northern Hispaniola and the Mona Passage in the 20th century (*ten Brink et al.*, 2011). Previous studies have established that only 2 large earthquakes are historically known to have occurred in the assumed location of the Puerto Rico Trench in 1785 and 1787 with an estimated magnitude of M8-8.25 for the latter date (*ten Brink et al.*, 2011; *McCann*, 1985). More recently, the 1918 earthquake of 7.3 in the Mona Canyon (Figure 1) generated a tsunami that impacted the western coast of Puerto Rico and was responsible for the loss of more than 100 lives (*Doser et al.*, 2005; *Mercado and McCann*, 1998).

The PRVI microplate was thought to be capable of producing earthquakes of estimated magnitudes of at least 8 with commensurate shaking and tsunamis risks to the population centers on the island (*McCann*, 1985). Risk assessment studies have also pointed out that the recurrence interval for a fully coupled subduction zone is of 67-125 years to generate a M 7.5 earthquake in the subduction region that covers Hispaniola, Puerto Rico and the Lesser Antilles (*Geist and Parsons*, 2009). More recently a study argued that the Puerto Rico Trench megathrust may be unable to generate great earthquakes (magnitude 8 and higher), although smaller shallow earthquakes could still be damaging (*ten Brink and López-Venegas*, 2012). Even though the characterization of the coupling in the trench was limited due to the lack of offshore GPS stations, the existing evidence supported the notion that the subduction zone north of Puerto Rico is not fully coupled. Other studies have shown that the potential magnitudes of earthquakes in the intra-arc are smaller than those in the subduction zone, but the shallow depths and proximity to the population increases their seismic risk (*ten Brink et al.*, 2011). However, one could also argue that patches that have been coupled for hundreds to thousands of years could also cause very destructive earthquakes (e.g. *Satake and Atwater*, 2007). Investigation and characterization of these regions is therefore important within the context of understanding the hazard in order to better prepare for the future.

Recent seismic activity has been dominated by the Indios sequence that began in December 2019 in the southwestern region of Puerto Rico and (Figure 1), generating large ground shaking that had not been felt since the 1918 (M 7.3) earthquake. The biggest earthquakes in the sequence (M5.0-6.4) caused substantial damage to structures in the south of the island, power outages, many injuries, and one confirmed death (*López-Venegas et al*., 2020). The continuation of seismicity at high levels for several weeks with several jumps in rate and magnitude created pervasive anxiety throughout the island population about what might happen next. The Indios sequence began in earnest on December 28 and the region remained active over a year later (*Van Der Elst et al.,* 2020). The Indios sequence has included more than 10 earthquakes of M>=5, with an apparent mainshock of M6.4 on January 7th, 2020. This sequence is particularly interesting to study because it presents a mix of both mainshock-aftershock (MS-AS) and swarm characteristics: the largest event happened later in the sequence providing evidence for swarm behavior but several MS-AS sequences with prominent Omori decay were embedded within it. Structurally, the earthquakes of M5.7 and M5.8 from January 6th and 7th happened on two E-SE striking, almost vertical, left lateral strike-slip faults (*Vičič et al.,* 2021). Interestingly, the M5.8 aftershock happened on a parallel fault that has almost the same strike as where the mainshock happened, potentially representing activation of a fault network. *Vičič et al.* (2021) also suggested that sequence happened in response to a tectonic transient that would be related to a slow slip episode associated with the Muertos Trough subduction. Therefore, more detailed temporal analysis of the Indios sequence seismicity has the potential to help us understand the nature of this apparently unusual sequence.

Motivated by our examination of the temporal patterns in the Indios sequence, this study also investigates previous sequences of increased seismicity rate throughout the Puerto Rico Seismic Network (PRSN) catalog, to help identify how anomalous the Indios sequence is. In particular, we sought to examine the relative prevalence of MS-AS sequences characterized by Omori or Bath's law patterns versus swarms that lack these temporal and magnitude patterns (*Mogi*, 1963; *Vidale and Shearer*, 2006; *Holtkamp and Brudzinski*, 2011). Previous research has suggested that swarms are prominent associated with the Puerto Rico Trench, but details are limited (*Pulliam et al*., 2007; *López-Venegas et al.,* 2009). The prevalence of swarms would be important because they present challenges for earthquake forecasting (*Llenos and Van der Elst*, 2019). A detailed characterization of previous aftershock and swarm sequences would provide critical input for forecasting efforts. In the case of swarms, characteristics of previous sequences would prove beneficial in forecasting the duration of or earthquake probabilities during swarms once they start happening (*Llenos and Van der Elst*, 2019). Consequently, improved understanding of typical temporal and magnitude patterns based on a review of historical seismicity is a key component for better hazard mitigation in Puerto Rico.

II. Temporal Patterns of the Indios Sequence Based on Template Matching

During cases when the seismicity rate increases to unprecedented levels, it is not uncommon for more limited detection and characterization of smaller events near the detection threshold. Due to the swarm-like nature of the sequence and knowing the importance of such small events to characterize the type of sequence, we employed three-station template matching to improve the detection of smaller seismicity and better understand the temporal patterns of the sequence (e.g., *Skoumal et al*., 2014). This preliminary analysis was focused on maximizing the real detections and reducing the detection of noise. Approximately 20,000 matches were found in the first 3 weeks of the sequence using roughly 2,000 cataloged events as templates. The best results were achieved using templates with seismograms from stations

MLPR (Magüeyes Lab, PR), CRPR (Cabo Rojo, PR) and AOPR (Arecibo Observatory, PR) (triangles, Figure 1), because these generated the least number of false positives, and their signal-to-noise ratio was better than other stations in the surrounding network. The magnitude of the events was calculated using the Richter approach where the amplitude recorded is used to estimate the magnitude based on the established relationship from the existing catalog of reported magnitudes (e.g., *Skoumal et al*., 2014).

The cataloged events in Figure 2A represent all of the template events used in the analysis. These events display a clear reduction of seismicity starting on January 2, 2020, that was suspicious given the lack of events below M 2.0. We estimated the magnitude of completeness (M_c) of the original template catalog to be 2.4 using the maximum curvature technique (Wiemer and Wyss, 2000), but there is an abrupt change from a M_c of 1.8 prior to Jan. 2, 2020, to M_c of 2.4 afterward based on a change in the network's capacity to catalog during a major sequence (PRSN, pers. comm.). Nevertheless, examining the rate of events with magnitudes greater than M2.4 (red, Figure 2A), the reduced seismicity rate between Jan. 2 and 6 is still noticeable. Moreover, the seismicity rate after larger earthquakes on Jan. 6 and 7 is surprisingly only slightly higher than that in late 2019.

Template matching provides an opportunity to investigate these temporal trends, with Figure 2B showing the detected earthquakes and rates of events greater than M 2.4 and Figure 2C showing the detected magnitudes and rates from M 1.0 to M 2.4. For our matched event catalog, the overall estimated M_c is 1.0, and in this case, the completeness changes from 0.7 to 1.1 when the activity increases on Jan 6, 2020. It should be noted that the M_c of a catalog constructed with template matching is generally thought to be biased due to the limited distribution of the template events (e.g., Skoumal et al., 2020), but it can still be useful for characterizing the detection limit of events similar to the templates. When considering both Figure 2B and 2C, we found a reduction in seismicity rate in 2020, but it does not occur until January 4-5 and the reduction is more modest. These plots also confirm there is a significantly higher seismicity rate after the large earthquakes on January 6 and 7. Overall, the template matching results are interesting because they show that smaller magnitude events exhibit swarm characteristics while events of greater magnitudes present more MS-AS patterns. For example, the rate of smaller seismicity in Figure 2C shows a more limited decay with time after the larger earthquakes compared to the more pronounced decays observed in the rate of larger seismicity (Figure 2B). This mixture of swarm and MS-AS behavior is intriguing and motivated us to review previous seismicity in the Puerto Rico region to investigate how common this behavior is.

III. Characterizing Swarms and Aftershock Sequences in the PRSN Catalog from 1986-2019

The data consists of all the earthquakes in the PRSN catalog from 1986 up until the Indios seismic sequence at the end of 2019. *Vičič et al.* (2021) suggested a small foreshock swarm sequence occurred in July 2019 but we found no evidence of this in the PRSN catalog. We geographically divided over 70,000 earthquakes in the PRSN catalog into the 4 quadrants for the island (NE, NW, SE, SW) given the proximity of these events to the PRSN stations (*Clinton et al*., 2006; *Huérfano et al*., 2018), but then added 2 additional regions further offshore approaching the trench where seismicity was particularly prevalent (NNE, NNW) (Figure 1).

In order to effectively process the seismicity in each geographic region, we developed an algorithm based on the weekly seismicity rate (Figure 3). This approach compared the seismicity rate of each week to that of the 3 previous weeks, looking for an increase that exceeds a factor of 4.5. We investigated a variety of threshold values from 0.5 to 5 and selected 4.5. Smaller values generated more false positives (gradual changes in seismicity rate that did not have well-defined initiations) and larger values would not detect smaller clusters of seismicity that could be visually confirmed as true MS-AS or swarm sequences. All detected sequences were initially saved from the beginning of the week when the seismicity level rises until the end of the second consecutive week where the activity level returned to the average weekly background seismicity rate (Figure 3B). The duration was then trimmed to be from the first earthquake to the last earthquake within this time frame (Figure 3C).

Our study has both similarities and differences to previous efforts to characterize swarms relative to MS-AS sequences. We sought to develop an automated sequence detection algorithm, which has the same goal as Vidale and Shearer (2006), but our catalog has a much smaller number of events due to the higher magnitude of completeness and much higher location uncertainty due to the lack of double-difference relocation being applied. So we used broader time and location thresholds than Vidale and Shearer (2006) (i.e., 2 km radius and 28-day windows). Our approach of detecting sequences based on increased seismicity rate is similar to that of Holtkamp and Brudzinski (2011), but we sought to develop an automated detection algorithm to increase objectivity when compared to typical manual detection approaches (e.g., Holtkamp and Brudzinski, 2011; Roland and McGuire, 2009). Several recent automated detection algorithms have been focused on swarm detection and would be biased against MS-AS detection (e.g., Reverso et al., 2016; Nishikawa and Ito, 2017).

The algorithm detected 70 sequences across the different geographic regions, with 59 sequences having at least 10 earthquakes. We found it difficult to classify sequences with less than 10 earthquakes, so we decided not to use them in the current study, hoping to improve their characterization with waveform correlation techniques in future work (*Skoumal et al*., 2015; *Skoumal et al*., 2016). To ensure all the events in a detected sequence were occurring at a similar location within a geographic region that could extend larger than 100 km wide (Figure 1), we calculated the median location of the cluster and the distance of each event from the median. To take into account location uncertainty, particularly for offshore and older sequences, we allowed events to be included in the sequence up to 20 km from the median location (Figure 3D). This step helps ensure events in the sequence are in roughly the same geographic location and did not occur in more disparate parts of our geographic boxes.

The trimmed and filtered sequences were then manually verified and classified into swarm or mainshock-aftershock (MS-AS) groups using criteria established in previous research (*Mogi*, 1963; *Holtkamp and Brudzinski*, 2011). Swarms were determined when the sequence did not show a clear mainshock at the beginning of the cluster, had a more constant seismicity rate during the sequence, and when the seismicity terminated more abruptly (Figure 4A). In contrast, MS-AS were identified when a clear mainshock at least 0.5 magnitude units higher than other big events in the cluster was observed (Bath's Law) as well as a clear decay of seismic activity following Omori's law that did not show an abrupt termination of the sequence (Figure 4B). We decided on 0.5 as the minimum threshold based on a relatively clear difference between the MS-AS and swarms in our dataset. The mean magnitude difference for swarms was 0.1 and for MS-AS it was 0.93, and the standard deviation for swarms was 0.09 and for MS-AS it was 0.57. Specifically, the MS-AS sequences produced a magnitude difference ranging from 0.40 to 2.16, while the swarms ranged from 0.0 to 0.36. Our characterization of the 59 sequences resulted in 40 swarms and 19 MS-AS sequences (Table S1).

IV. Relationships Between Swarms and Mainshock-Aftershock (MS-AS) Sequences in the PRSN Catalog

Using previous research as a guide (*Vidale and Shearer*, 2006; *Holtkamp and Brudzinski*, 2011; *Skoumal et al.,* 2015), we reviewed our swarm and aftershock sequences on a plot that shows the largest earthquake versus the number of events in the sequence (Figure 5). This plot is designed to create a separation between the two types of sequences. Because swarms normally have more events per largest event magnitude they would be plotted on the top left corner and MS-AS would normally have fewer events per largest magnitude and would be plotted on the bottom right corner of the plot (*Vidale and Shearer*, 2006).

In Figure 5A, swarms generally had larger numbers of events per maximum magnitude, but plenty of overlap between swarms and MS-AS is visible. In order to investigate the cause of the overlap, we restricted the plot to only recent sequences to see whether the increased number of seismometers in the PRSN would result in a more definitive characterization (*Clinton et al*., 2006; *Huérfano et al*., 2018). Plotting only clusters since 2010 illustrates a better separation (Figure 5B), and we also note that the number of events per sequence is higher on average for these recent sequences. This indicates the increased number of seismometers lowered the magnitude of detection so that more smaller magnitude events can be detected for each sequence, providing a larger number of events to help discern between swarms and MS-AS characteristics.

The process of manually characterizing the sequences also led us to consider if some of the overlap in Figure 5A was due to sequences having a mix of both swarm and MS-AS behavior. We decided to recharacterize the sequences to include 3 additional categories: 1) swarms followed by a MS-AS (Figure 6A), initially characterized as a swarm, but with a prominent MS-AS during the swarm, 2) MS-AS followed by a swarm (Figure 6B), initially characterized as a MS-AS based on the prominent initial mainshock, but lacking signatures of a typical Omori decay, and 3) MS-AS followed by another MS-AS (Figure 6C), initially characterized as a MS-AS, but with a second prominent MS-AS occurring soon after the initial one. We found 7 cases of a Swarm followed by a MS-AS, 2 cases of a MS-AS-followed by Swarm, and 8 cases of a MS-AS followed by a MS-AS (Table S1). To help justify why we considered these multiple behaviors as single sequences, we found that only 7 sequences with swarm-like behavior were identified during 1990-2009 in the NNE region and 2 of them occurred as Swarms followed by MS-AS group. This indicates that swarms were not particularly prevalent during that time period in that region, such that a swarm occurring days after a MS-AS is unlikely to occur by coincidence. The prevalence of these mixed sequences (29% of all sequences) indicates they are relatively common in Puerto Rico. Figure 5C shows the mixed sequences primarily occur in the overlap between the swarms and MS-AS, suggesting that the prevalence of mixed sequences is contributing to the more extensive overlap than in previous studies. In previous studies that have identified a few examples of mixed sequences (e.g., *De Barros et al.,* 2019; *Bachura et al.,* 2021), the mixture is thought to occur when multiple fault segments are activated with local variations of fault rheology, smoothness, differential stress, or fluid circulation.

To further clarify the nature of our detected sequences, we determined the number of foreshocks as the number of events before the largest earthquake in each sequence and calculated what percentage of the sequence was foreshocks. On average, foreshocks of an MS-AS made up only 3.5% of the sequence. In contrast, swarms had 49% foreshocks on average, consistent with the idea that the largest event occurs with an equal likelihood in time within a swarm sequence (e.g., Vidale and Shearer, 2006). For the 8 MS-AS followed by MS-AS sequences, 5 had small foreshock percentages (0-2.8%) due to the larger mainshock occurring in the first group, while 3 had larger foreshock percentages (17%-68.7%) due to the larger mainshock occurring in the second group. Intriguingly, the magnitude difference between the 2 mainshocks for all 8 of these sequences was less than or equal to 1.0 with most less than 0.1. This is a key reason we prefer to refer to these sequences as MS-AS followed by MS-AS as opposed to foreshock-mainshock-aftershock sequences.

One more possibility we considered is that variations in duration could influence how sequences are represented in these plots. To account for this, we normalized the number of events by a unit of time (per week) in Figure 5D. This generates some additional separation as the swarms tended to have higher seismicity rates when compared to MS-AS, but plenty of overlap remains, indicating this factor alone cannot account for the overlap between the swarm and MS-AS distributions.

V. Temporal Patterns of Swarms and Mainshock-Aftershock Sequences in the PRSN Catalog

Based on the findings in Figure 5D, we began our investigation of the temporal patterns of the detected sequences by focusing on the duration of the different sequence types. Figure 7 is a log-log plot showing the number of events versus the duration of the sequences. This plot highlights how the MS-AS tends to last longer than the swarms, with only MS-AS sequences extending longer than 20 days and only swarms lasting shorter than 1 day. We also found a much stronger relationship between the number of events and the duration for MS-AS than for swarms. A relationship is expected for MS-AS as a sequence with more events (presumably due to a larger mainshock) is typically going to have a longer aftershock sequence. However, we also expected to see a strong relationship for swarms, as swarms tend to have a relatively constant rate of seismicity over time, such that longer sequences should have more events. The lack of a strong demonstration of this in Figure 7 indicates differences in the seismicity rate for shorter swarms (higher rate) versus longer swarms (lower rate) which could offset the expected trend. If this trend can be verified over a larger population of swarms, it could provide some clues about the causes of swarms. For example, if swarms are driven by deformation associated with slow slip episodes (e.g., *Hirose et al.,* 2008; *Passarelli et al.,* 2021), it suggests that slow slip may have variable deformation rates that are related to the duration of the episodes.

To further understand the MS-AS behavior, we used log-log plots to look for patterns in aftershock decay rates (Figure 8A). These plots show the seismicity rate versus the time after the largest event in the sequence. The slope approximates the p-value, a constant from Omori Law that describes the decay of aftershocks over time (e.g., *Utsu et al.*, 1995). Although there is considerable debate about what controls the p-value of a sequence, it may be related to stress conditions, temperature of the crust, the structural heterogeneity, and fluid-driven permeability dynamics (e.g., *Enescu and Ito*, 2002; *Miller*, 2020). We sought to characterize the p-values for sequences in our study to look for any coherent patterns. The uncertainties of the p-values were calculated through bootstrapping by removing 10% of the events and recalculating the p-value

100 times to generate a mean p-value and standard deviation to represent the uncertainty. The average uncertainty in p-value for our sequences is 0.03. In order for a sequence to be considered in the p-value analysis, the number of events after the largest earthquake had to be at least 10, there had to be a rate estimate in at least 5 time bins, and the uncertainty standard deviation had to be 0.10 or less. We attempted calculating p-values with several different magnitudes thresholds but did not find that the p-values changed substantially until the sequence fell below our consideration thresholds.

We identified that the different types of sequences had different p-values (Figure 8). Traditional MS-AS had an average p-value of 0.9, at the lower end of the expected range (0.9-1.5) (*Utsu et al.*, 1995). We also found that MS-AS followed by MS-AS had a similar average of 0.9, indicating that the aftershock decay rate was similar to single MS-AS sequences despite their doublet nature. The Swarm followed by MS-AS sequences also had an average of 0.9, but this group had a wider diversity and had two cases with p-values less than 0.7 when there the swarm activity continued to be productive after the mainshock occurred. MS-AS followed by Swarms showed this pattern even more clearly. Finally, swarms had an average p-value of 0.6, consistent with the typical lack of Omori decay used to characterize a swarm sequence . We note that Enescu et al. (2009) utilized superposition to combine sequences based on ETAS productivities to group sequences that are more swarm-like versus those more like MS-AS. They found that the swarm group had a lower p-value (0.7) than the MS-AS group (0.9), although they noted that forming sequences via superpositions tends to produce lower p-values (e.g., Utsu et al., 1995). Since we estimated p-values of individual sequences without the need for superposition, we can more confidently say that the p-values of swarms and mixed sequences are lower than those of MS-AS. The generally lower p-values of mixed sequences suggests that p-values are modulated by the amount of swarm-like behavior present in the type of sequence in the Puerto Rico region. Considering that swarms are often considered to be associated with fluid fluxes, this could support the fluid-driven permeability conceptual model suggested by *Miller* (2020).

VI. Geographics Patterns of Swarms and MS-AS Sequences in the PRSN Catalog

Figure 9 shows the geographic pattern of the various sequences detected in this study. The initial rate detection algorithm only identified 3 potential sequences in the NE and NW regions, but these were discarded based on the low number of events (<10 earthquakes) in those sequences. The lack of sequences that met our criteria in the NE region is not surprising considering this region had the lowest seismicity rate (1861 events, with 614 events M>3) (Figure 9). The NW region does have a higher seismicity rate (3018 events, 711 with M>3) with two prominent areas of more pronounced seismicity (Figure 9), and yet our algorithm did not detect temporal increases that met our criteria to be defined as sequence. The NNE and NNW regions had higher seismicity rates (4998 and 6120 events, respectively; 2718 and 2382 with M>3), and these correspond to the regions with the most detected sequences (24 and 20 sequences, respectively). Intriguingly, the SE region has a lower seismicity rate (3770 events, 696 with M>3) approaching that of the NW region, but there were 9 sequences detected in the SE region. Even more surprising is that the SW region has had the highest seismicity rate even prior to the Indios sequences (8563 events, 969 with M>3), but only had 6 sequences detected. The relatively small number of sequences detected suggests the changes in seismicity rate have tended to be more gradual in the SW region prior to the Indios sequence than in the NNE, NNW, and SE regions.

We should be careful to note that the ability to detect sequences has been variable over space and time due to the changing M_c throughout the PRSN catalog (*Clinton et al*., 2006; *Huérfano et al*., 2018). We calculated the M_c for each of our study regions: SW = 2.0, SE = 2.2, NW = 2.6, NE = 2.8, NNW = 2.8, and NNE = 3.1. The eastern side of our study area has a slightly higher M_c than the western side, but a more pronounced pattern is the increase in M_c

from south to north that creates an artificially lower number of events per sequence offshore. However, a smaller magnitude of completeness in recent times due to increased recordings creates more events per sequence and more sequences. These biases prevent a simple effective metric to distinguish when combining sequences across the various geographic regions and time frames. The use of template matching in the recent Indios seismic sequence proved to be very effective when looking for smaller magnitude events that improve the magnitude of completeness, making it easier to identify the characteristic behavior of this sequence. This suggests that future work should focus on more extensive template matching of the PRSN catalog to increase detection associated with the sequences we investigated and potentially can lead to a larger catalog of sequences.

Given the catalog of sequences that was produced, we observed some general spatial patterns in the Puerto Rico region. We observed that the sequences in the southern part of the island tend to follow crustal faults and are generally shallower than the sequences in the northern region. Some of the northern sequences occur in the vicinity of the 19N fault zone, but most northern sequences are deeper, more distributed, and appear to be associated with the subduction interface (Figure 9 and Table S1). Northern sequences tend to have more events and more sequences in general when compared to the southern sequences, despite the fact that the land based PRSN enables a smaller magnitude of detection in the southern regions (*Clinton et al*., 2006; *Huérfano et al*., 2018), suggesting this disparity is likely even more pronounced if recording was comparable. The limited number of sequences in the south makes it difficult to identify more specific patterns on the island.

To interpret our findings of many sequences offshore with pervasive swarm activity, we turned our attention to prior analyses of subduction zone earthquake swarm studies. Previous research has indicated that swarms appear to occur in regions of reduced coupling (*Holtkamp and Brudzinski*, 2014). This finding was based on reviewing a global compilation of megathrust earthquake swarms (*Holtkamp and Brudzinski*, 2011), and comparing them to the extent of several dozen great megathrust earthquake rupture zones and geodetic estimates of subduction interface coupling. Earthquake swarm activity in places like Japan, Chile, Sumatra, and Alaska correlated with regions on the plate interface that show low seismic coupling, in between the rupture zones of great earthquakes. The swarms appear to represent areas of high-stress heterogeneity and low overall coupling that creates an obstacle for large earthquake rupture. Given that 34 of the 40 swarm sequences we found were in the northern offshore subduction zone and were distributed over a broad region (Figure 9), we argue that the subduction interface in Puerto Rico has relatively low coupling due to heterogeneous stress. The findings of *Holtkamp and Brudzinski* (2011) indicate the pervasive swarms would make it unlikely that a large, coupled patch would rupture as a great megathrust earthquake. This supports the conclusions of *ten Brink and López-Venegas* (2012) that great megathrust earthquakes are unlikely to happen on the subduction interface based on GPS data indicating weak coupling on the subduction interface. However, it is important to note that this interpretation does not preclude shallow earthquakes reaching into the magnitude 7 sizes occurring and generating damage (*ten Brink and López-Venegas*, 2012). Strong (M6-6.9) and major (M7-7.9) sized earthquakes could still be very disruptive for population centers close to the subduction interface.

VII. Conclusions

Our study was motivated initially by the unexpected seismic behavior observed in the Indios sequence. Template matching was employed in order to better characterize and understand it. This approach improved the detection of smaller seismicity, and we were able to observe the temporal patterns of the sequence and how it varied depending on the magnitude threshold. We observed that smaller magnitude events exhibit swarm characteristics while events of greater magnitudes present more mainshock-aftershock (MS-AS) patterns. Then in an effort to understand the mixture of the swarm and MS-AS behavior in the sequence we used an algorithm to study all previous sequences. Employing the seismicity rate detection algorithm and sequence classification characterization criteria, we found 40 swarms and 19 MS-AS sequences of increased seismicity rate in the PRSN catalog. 58% of the sequences follow traditional swarm patterns and 14% adhere to traditional MS-AS behavior while 29% of the sequences have both swarm and MS-AS behaviors. Therefore, it is not unexpected for the 2020 SW Puerto Rico sequence to have a mixture of both characteristics.

We also found that the duration of MS-AS is proportional to the number of events as it would be expected, and swarms tend to have shorter durations and no distinctive pattern relative to the number of events in the sequence. Consequently, we evaluated the P-values for the different sequences and found that the P-value decreases depending on the amount of swarm-like behavior in the sequence.

Additionally, we found evidence that supports the conclusion of *ten Brink and López-Venegas* (2012) that a great (M>8.0) megathrust earthquake on the subduction interface is unlikely given the amount of swarm activity in this region consistent with previous research that has suggested the subduction interface is weakly coupled.

Acknowledgments

Support for this work was provided by the Diversity Enhancement Pathway Graduate Assistantship from the Geology and Environmental Earth Science Department of Miami University. The manuscript benefited greatly from feedback provided by B. Currie, B. Colon, A. Llenos, C. Mcleod, M. Page, E. Vanacore and S. Fasola. A. Llenos and an anonymous reviewer provided constructive reviews that improved the quality of this study.

Data and Resources

The catalog of earthquakes analyzed in this study was retrieved from the Puerto Rico Seismic Network (http://www.prsn.uprm.edu/English/catalogue/index.php). Seismograms recorded by the PRSN were retrieved from the IRIS DMC to perform the 3 station template matching. Supplemental Material for this article consists of a table describing the characteristics of the earthquake sequences identified in this study.

References

Bachura, M., Fischer, T., Doubravová, J., & Horálek, J. (2021). From earthquake swarm to a main shock–aftershocks: the 2018 activity in West Bohemia/Vogtland. *Geophysical Journal International*, 224(3), 1835-1848.

Byrne, D.B., Suarez, G., McCann, W.R., 1985. Muerto Trough subduction-microplate tectonics in the northern Caribbean. *Nature* 317, 420-421

Calais, E., N. Béthoux, and B. M. de Lépinay (1992). From transcurrent faulting to frontal subduction: A seismotectonic study of the Northern Caribbean Plate Boundary from Cuba to Puerto Rico, *Tectonics* **11**, no. 1, 114–123, doi: https://doi.org/10.1029/91TC02364.

Chaytor, J. D., and U. S. ten Brink (2010). Extension in Mona Passage, Northeast Caribbean, *Tectonophysics* 493, no. 1, 74–92, doi: 10.1016/j.tecto.2010.07.002.

Clinton, J. F., Cua, G., Huérfano, V., von Hillebrandt-Andrade, C. G., & Cruzado, J. M. (2006). The current state of seismic monitoring in Puerto Rico. Seismological Research Letters, 77(5), 532-543.

De Barros, L., Baques, M., Godano, M., Helmstetter, A., Deschamps, A., Larroque, C., & Courboulex, F. (2019). Fluid-induced swarms and coseismic stress transfer: A dual process highlighted in the aftershock sequence of the 7 April 2014 earthquake (Ml 4.8, Ubaye, France). *Journal of Geophysical Research: Solid Earth*, 124(4), 3918-3932.

Dillon, W., U. T. Brink, A. Frankel, C. Mueller, and R. Rodriguez (1999). Seismic and tsunami hazards in northeast Caribbean addressed at meeting, *Eos, Transactions American Geophysical Union* **80**, no. 28, 309–310, doi: 10.1029/99EO00226.

Donnelly, T.W., 1989. Geologic history of the Caribbean and Central America. In: Bally, A.W., Palmer, A.R. (Eds.), An Overview, Geology of North America: A. Geological Society of America, Boulder, CO, pp. 299-321

Doser, D. I., C. M. Rodriguez, and C. Flores (2005). Historical earthquakes of the Puerto Rico–Virgin Islands region (1915–1963), in *Active Tectonics and Seismic Hazards of Puerto Rico, the Virgin Islands, and Offshore Areas*, Geological Society of America, doi: 10.1130/0-8137-2385-X.103.

Enescu, B., and K. Ito (2002). Spatial analysis of the frequency-magnitude distribution and decay rate of aftershock activity of the 2000 Western Tottori earthquake, *Earth Planet Sp* **54**, no. 8, 847–859, doi: 10.1186/BF03352077.

Enescu, B., Hainzl, S., and Ben-Zion, Y. (2009). Correlations of seismicity patterns in Southern California with surface heat flow data. *Bulletin of the Seismological Society of America*, 99(6), 3114-3123.

Geist, E. L., and T. Parsons (2009). Assessment of source probabilities for potential tsunamis affecting the U.S. Atlantic coast, *Marine Geology* **264**, no. 1–2, 98–108, doi: 10.1016/j.margeo.2008.08.005.

Granja Bruña, J. L., U. S. ten Brink, A. Muñoz-Martín, A. Carbó-Gorosabel, and P. Llanes Estrada (2015). Shallower structure and geomorphology of the southern Puerto Rico offshore margin, *Marine and Petroleum Geology* **67**, 30–56, doi: 10.1016/j.marpetgeo.2015.04.014.

Hirose, H., Matsuzawa, T., Kimura, T., & Kimura, H. (2014). The Boso slow slip events in 2007 and 2011 as a driving process for the accompanying earthquake swarm. *Geophysical Research Letters*, **41**(8), 2778-2785.

Holtkamp, S. G., and M. R. Brudzinski (2011). Earthquake swarms in circum-Pacific subduction zones, *Earth and Planetary Science Letters* **305**, no. 1–2, 215–225, doi: 10.1016/j.epsl.2011.03.004.

Holtkamp, S., and M. R. Brudzinski (2014). Megathrust earthquake swarms indicate frictional changes which delimit large earthquake ruptures, *Earth and Planetary Science Letters* **390**, 234–243, doi: 10.1016/j.epsl.2013.10.033.

Huérfano, V., C. von Hillebrandt-Andrade, and G. Báez-Sánchez (2005). Microseismic activity reveals two stress regimes in southwestern Puerto Rico, in *Active Tectonics and Seismic Hazards of Puerto Rico, the Virgin Islands, and Offshore Areas*, Geological Society of America, doi: 10.1130/0-8137-2385-X.81.

Huérfano, V. A., Vanacore, E. A., Martínez-Cruzado, J. A., Lopez, A. M., & Baez-Sanchez, G. (2018). Geophysical and Sea level data availability in Puerto Rico. In *AGU Fall Meeting Abstracts* (Vol. 2018, pp. S13D-0502).

Jansma, P. E., G. S. Mattioli, A. Lopez, C. DeMets, T. H. Dixon, P. Mann, and E. Calais (2000). Neotectonics of Puerto Rico and the Virgin Islands, northeastern Caribbean, from GPS geodesy, *Tectonics* **19**, no. 6, 1021–1037, doi: 10.1029/1999TC001170.

López-Venegas, A. M., J. Pulliam, U. ten Brink, H. E. Mintz, and C. von Hillebrandt-Andrade (2009), Deployment of ocean bottom seismometers south of Puerto Rico Trench yields new insights into the behavior of seismic swarms, Eos Trans. AGU, 90(52), Fall Meet. Suppl., Abstract T23B-1902.

López-Venegas, A.M., Hughes, K.S., & Vanacore, E. (2020), Puerto Rico's Winter 2019-2020 Seismic Sequence Leaves the Island On Edge, *Temblor*, http://doi.org/10.32858/temblor.064.

Llenos, A. L., and N. J. van der Elst (2019). Improving Earthquake Forecasts during Swarms with a Duration Model, *Bulletin of the Seismological Society of America* 109, no. 3, 1148–1155, doi: 10.1785/0120180332.

Mann, P., Taylor, F.W., Edwards, R.L., Kuc, T., 1995. Actively evolving microplate formation by oblique collision and sideways motion along strike–slip faults: an example from the northeastern Caribbean plate margin. *Tectonophysics* 246, 1-69.

McCann, W. R. (1985). On the earthquake hazards of Puerto Rico and the Virgin Islands, *Bulletin of the Seismological Society of America* **75**, no. 1, 251–262.

Meighan, H. E., Pulliam, J., ten Brink, U., & López-Venegas, A. M. (2013). Seismic evidence for a slab tear at the Puerto Rico Trench. *Journal of Geophysical Research: Solid Earth*, 118(6), 2915-2923.

Mercado, A., and W. McCann (1998). Numerical Simulation of the 1918 Puerto Rico Tsunami, *Natural Hazards* **18**, no. 1, 57–76, doi: 10.1023/A:1008091910209.

Miller, S. A. (2020). Aftershocks are fluid-driven and decay rates controlled by permeability dynamics. *Nature Communications*, 11(1), 1-11.

Mogi, K. (1963), Some discussions on aftershocks, foreshocks, and earthquake swarms: The fracture of a semi-infinite body caused by an inner stress origin and its relation to the earthquake phenomenon, *Bull. Earthquake Res. Inst. Univ. Tokyo*, 41, 615–658.

Nishikawa, T., & Ide, S. (2017). Detection of earthquake swarms at subduction zones globally: Insights into tectonic controls on swarm activity. *Journal of Geophysical Research: Solid Earth*, 122(7), 5325-5343.

Passarelli, L., Selvadurai, P. A., Rivalta, E., & Jónsson, S. (2021). The source scaling and seismic productivity of slow slip transients. *Science Advances*, 7(32), eabg9718.

Pulliam, J., V. A. Huérfano, U. ten Brink, and C. von Hillebrandt-Andrade (2007), Seismic sequences in the Sombrero Seismic Zone, *Eos. Trans. AGU*, 88(23), Jt. Assem. Suppl., Abstract S52A-02.

Reverso, T., Marsan, D., and Helmstetter, A. (2015). Detection and characterization of transient forcing episodes affecting earthquake activity in the Aleutian Arc system. *Earth and Planetary Science Letters*, 412, 25-34.

Roland, E., and J. J. McGuire (2009), Earthquake swarms on transform faults, *Geophys. J. Int.*, 178(3), 1677–1690, doi:10.1111/j.1365-246X.2009.04214.x

Satake, K.,and Atwater, B. F. (2007). Long-term perspectives on giant earthquakes and tsunamis at subduction zones. *Annu. Rev. Earth Planet. Sci.*, **35**, 349-374.

Skoumal, R. J., M. R. Brudzinski, B. S. Currie, and J. Levy (2014). Optimizing multi-station earthquake template matching through re-examination of the Youngstown, Ohio, sequence, *Earth and Planetary Science Letters* **405**, 274–280, doi: 10.1016/j.epsl.2014.08.033.

Skoumal, R. J., Brudzinski, M. R., & Currie, B. S. (2015). Distinguishing induced seismicity from natural seismicity in Ohio: Demonstrating the utility of waveform template matching. *Journal of Geophysical Research: Solid Earth*, 120(9), 6284-6296, doi:10.1002/2015JB012265.

Skoumal R. J., Brudzinski M. R., Currie B. S. (2016). An Efficient Repeating Signal Detector to Investigate Earthquake Swarms, *Journal of Geophysical Research: Solid Earth*, 121(8), 5880-5897, doi:10.1002/2016JB012981.

Skoumal, R. J., Brudzinski, M. R., Currie, B. S., & Ries, R. (2020). Temporal patterns of induced seismicity in Oklahoma revealed from multi-station template matching. *Journal of Seismology*, 24(5), 921-935.

ten Brink, U. (2005), Vertical motions of the Puerto Rico Trench and Puerto Rico and their cause, J. Geophys. Res., 110, B06404, doi:10.1029/2004JB003459.

ten Brink, U., W. H. Bakun, and C. H. Flores (2011). Historical perspective on seismic hazard to Hispaniola and the northeast Caribbean region, *Journal of Geophysical Research: Solid Earth* 116, no. B12, doi: https://doi.org/10.1029/2011JB008497.

ten Brink, U., and A. M. López-Venegas (2012). Plate interaction in the NE Caribbean subduction zone from continuous GPS observations, *Geophysical Research Letters* **39**, no. 10, doi: https://doi.org/10.1029/2012GL051485.

Utsu, T., Y. Ogata, R. S, and Matsu'ura (1995). The Centenary of the Omori Formula for a Decay Law of Aftershock Activity, *J. Phys. Earth*, 43, no. 1, 1–33, doi: 10.4294/jpe1952.43.1.

Van Der Elst, N., J. L. Hardebeck, and A. J. Michael (2020). Potential duration of aftershocks of the 2020 southwestern Puerto Rico earthquake, USGS Numbered Series 2020–1009, U.S. Geological Survey, Reston, VA, Open-File Report, doi: 10.3133/ofr20201009.

Vidale, J. E., and P. M. Shearer (2006). A survey of 71 earthquake bursts across southern California: Exploring the role of pore fluid pressure fluctuations and aseismic slip as drivers, *Journal of Geophysical Research: Solid Earth* **111**: B5, doi: 10.1029/2005JB004034.

Vičič, B., S. Momeni, A. Borghi, A. Lomax, and A. Aoudia (2021). The 2019-2020 Indios, Puerto Rico earthquake sequence: seismicity and faulting, https://eartharxiv.org/repository/view/2265/

Wiemer, S., & Wyss, M. (2000). Minimum magnitude of completeness in earthquake catalogs: Examples from Alaska, the western United States, and Japan. Bulletin of the Seismological Society of America, 90(4), 859-869.

Full Mailing Addresses

Wilnelly Ventura-Valentin and Michael R. Brudzinski
Department of Geology and Environmental Earth Science
Miami University
250 S. Patterson Avenue
Oxford, OH 45056

Figure Captions

Figure 1. Map of the study area around Puerto Rico. White boxes show the 6 different regions we investigated for swarm and mainshock-aftershock (MS-AS) seismic sequences. Green triangles show the locations of seismic stations used for template matching of the Indios earthquake sequence. Stars represent historical large seismicity, with the largest highlighting the Indios seismic sequence; stars accompanied by question marks mean that their location is assumed and not exact. Curved white lines show mapped faults (Courtesy E. Vanacore).

Figure 2. Summary of 3-station template matching results for the early part of the 2019-2020 Indios earthquake sequence, showing earthquake magnitudes (circles) and rates (red line). The PRSN catalog (A) was used as template events (blue), and the rate shown is for magnitudes greater than 2.4. Matched events (black) are shown in the other two panels highlighting the rate for earthquakes with magnitudes larger than 2.4 (B) and between 1.0 and 2.4 (C).

Figure 3. Illustration of how the algorithm finds the sequences that overcome the threshold of background seismicity. The plot shows earthquakes per week (A) and the magnitude of events (B) per time in days. C shows the magnitude over time of a set of events that then is filtered by distance over time (D).

Figure 4. Examples of a (A) swarm sequence (B) MS-AS sequence.

Figure 5. For each sequence, the symbol location indicates the maximum earthquake magnitude in the sequence versus the number of events in the sequence (A, B, and C) or the number of events per week (D). B shows sequences since 2010. Symbol shape indicates our sequence classification: A-B shows the initial characterization of swarms and MS-AS and C-D show the additional determination of mixed sequences.

Figure 6. Examples of the additional classifications we used to describe mixed sequences that were more complicated and had multiple characteristics.

Figure 7. Duration in days of the sequence versus the number of events in the sequence. Red indicates sequences that were nominally swarms and blue indicate sequences that had predominantly MS-AS patterns. Symbol shape indicates the more detailed classification.

Figure 8. Estimation of the Omori p-value for sequences detected in this study. (A) Log-log plots of the seismicity rate versus the time after the largest event in the sequence for examples of 4 different sequence types. (B) Estimated p-values of the different types of sequences (colored symbols). The symbol size matches the average standard deviation of the p-value to aid in interpretation of these values.

Figure 9. Map of area of study with all cataloged seismicity from PRSN in black. Thick white lines indicate the specific subdivision within the study (Figure 2). Regions outlined in green (MS-AS) or yellow (swarm) indicate the 1-sigma spatial distribution enclosing ⅔ of the events in the sequence on average. Thin white lines show mapped faults (Courtesy of E. Vanacore).

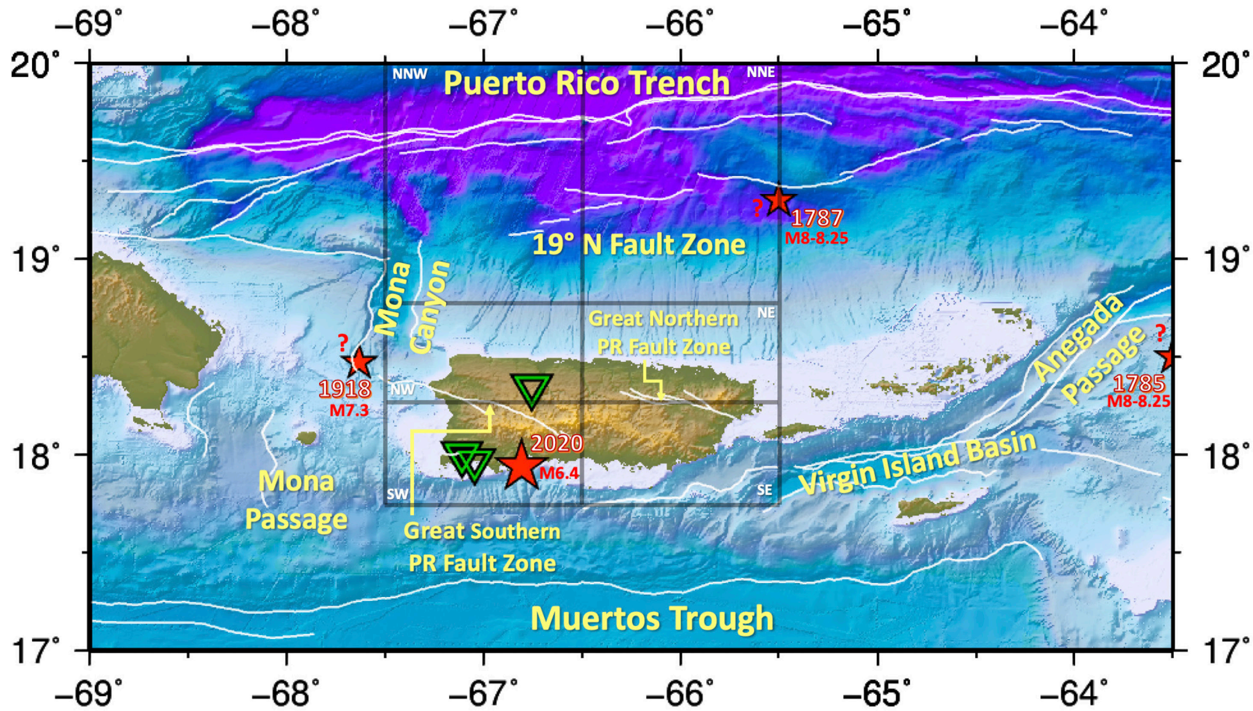

−69˚
−68˚
−67˚
−66˚
−65˚
−64˚
20˚
19˚
18˚
17˚
NNW
NNE
Puerto Rico Trench
?
1787
M8-8.25
19° N Fault Zone
Mona
Canyon
Great Northern
PR Fault Zone
NE
NW
?
1918
M7.3
2020
M6.4
SW
SE
Mona
Passage
Great Southern
PR Fault Zone
Virgin Island Basin
Anegada
Passage
?
1785
M8-8.25
Muertos Trough

Figure 1. Map of the study area around Puerto Rico. White boxes show the 6 different regions we investigated for swarm and mainshock-aftershock (MS-AS) seismic sequences. Green triangles show the locations of seismic stations used for template matching of the Indios earthquake sequence. Stars represent historical large seismicity, with the largest highlighting the Indios seismic sequence; stars accompanied by question marks mean that their location is assumed and not exact. Curved white lines show mapped faults (Courtesy E. Vanacore).

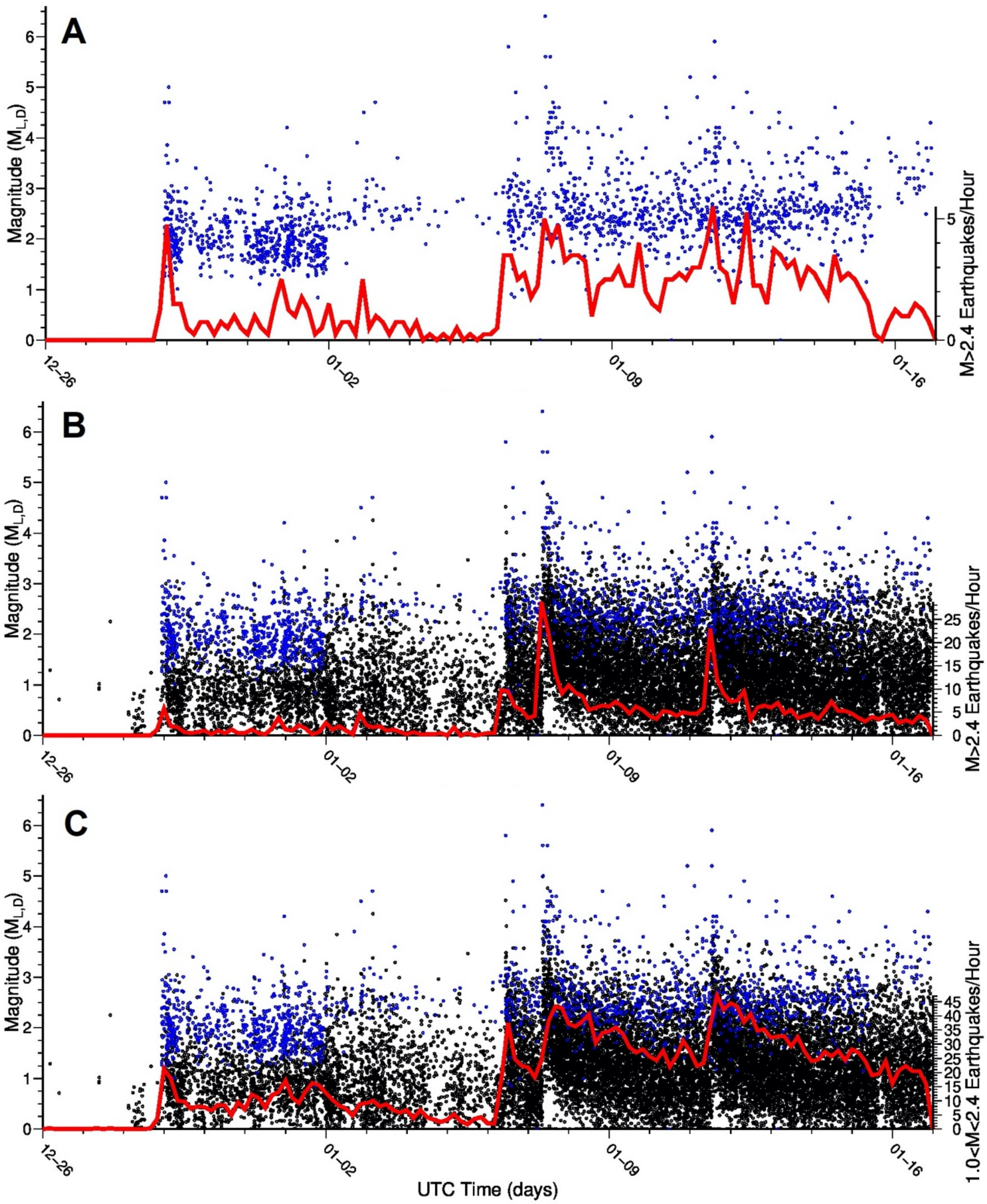

Figure 2. Summary of 3-station template matching results for the early part of the 2019-2020 Indios earthquake sequence, showing earthquake magnitudes (circles) and rates (red line). The PRSN catalog (A) was used as template events (blue), and the rate shown is for magnitudes greater than 2.4. Matched events (black) are shown in the other two panels highlighting the rate for earthquakes with magnitudes larger than 2.4 (B) and between 1.0 and 2.4 (C).

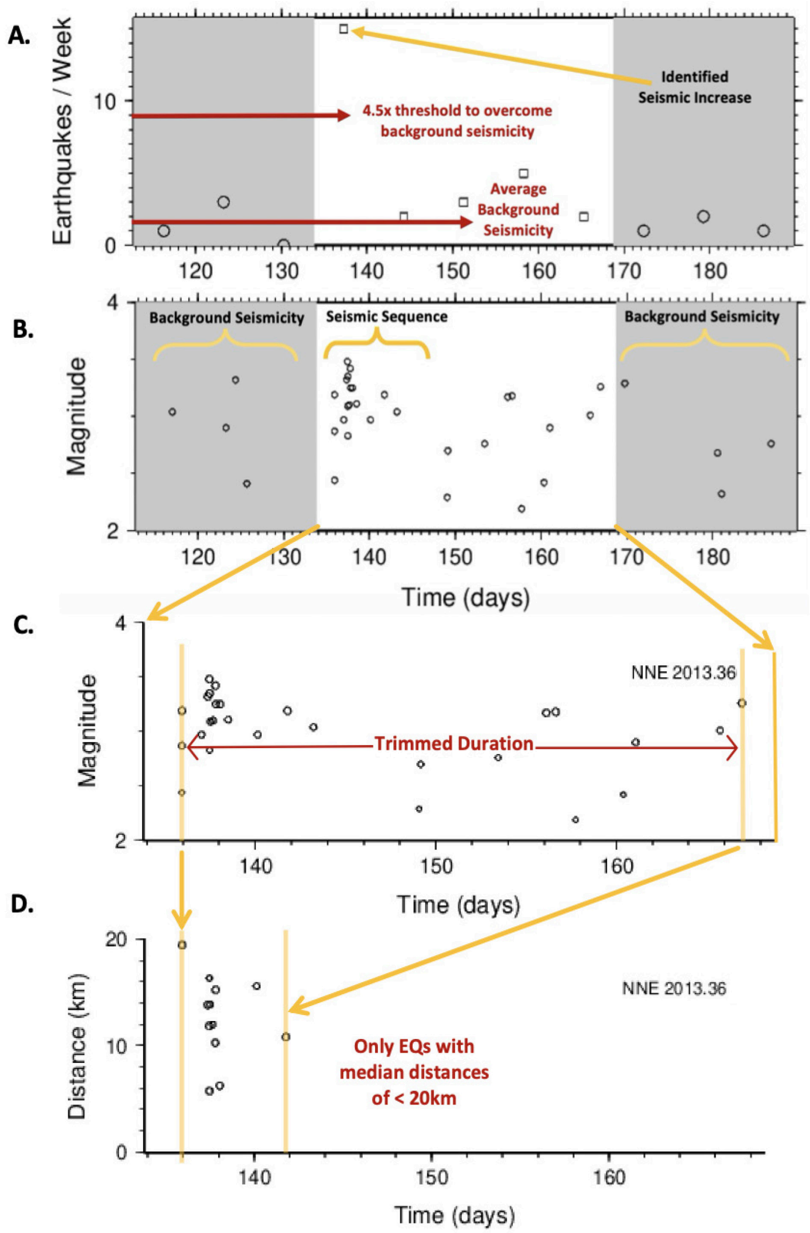

Figure 3. Illustration of how the algorithm finds the sequences that overcome the threshold of background seismicity. The plot shows earthquakes per week (A) and the magnitude of events (B) per time in days. C shows the magnitude over time of a set of events that then is filtered by distance over time (D).

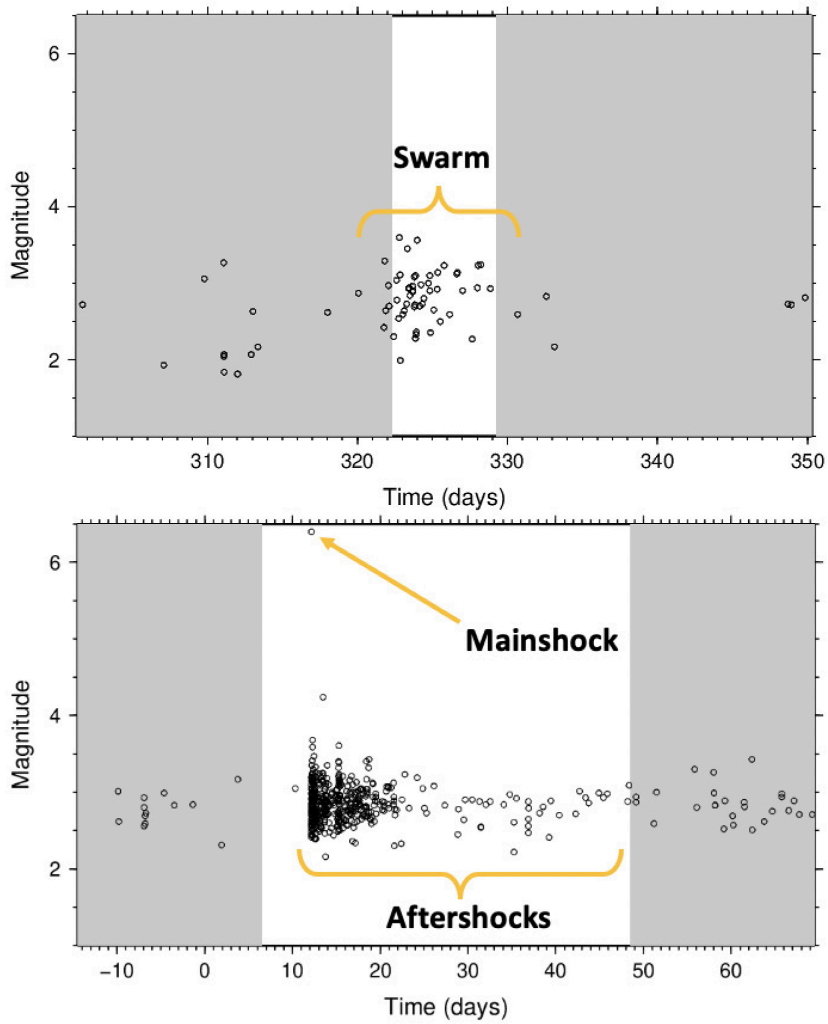

Figure 4. Examples of a (A) swarm sequence (B) MS-AS sequence.

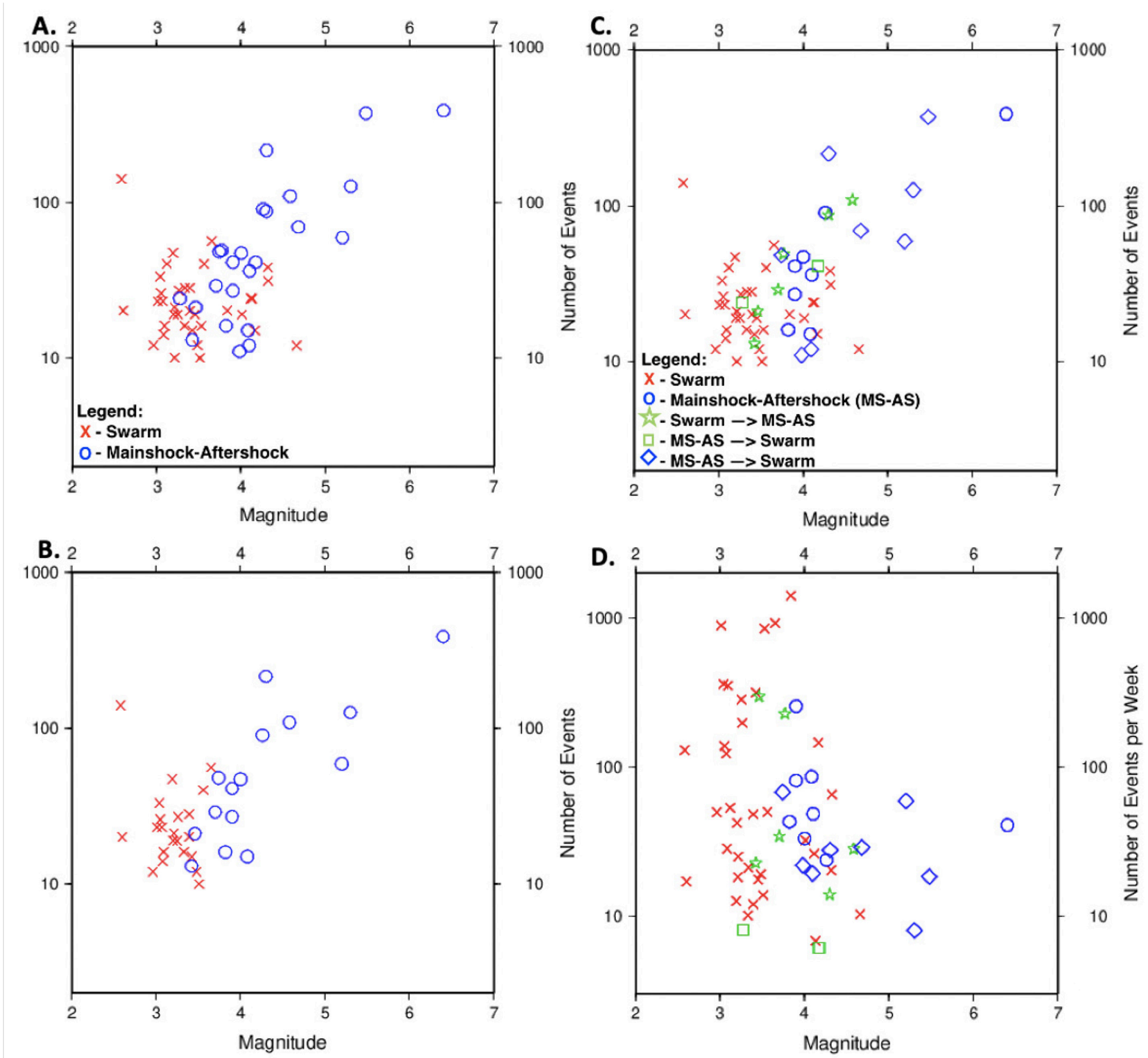

Figure 5. For each sequence, the symbol location indicates the maximum earthquake magnitude in the sequence versus the number of events in the sequence (A, B, and C) or the number of events per week (D). B shows sequences since 2010. Symbol shape indicates our sequence classification: A-B shows the initial characterization of swarms and MS-AS and C-D show the additional determination of mixed sequences.

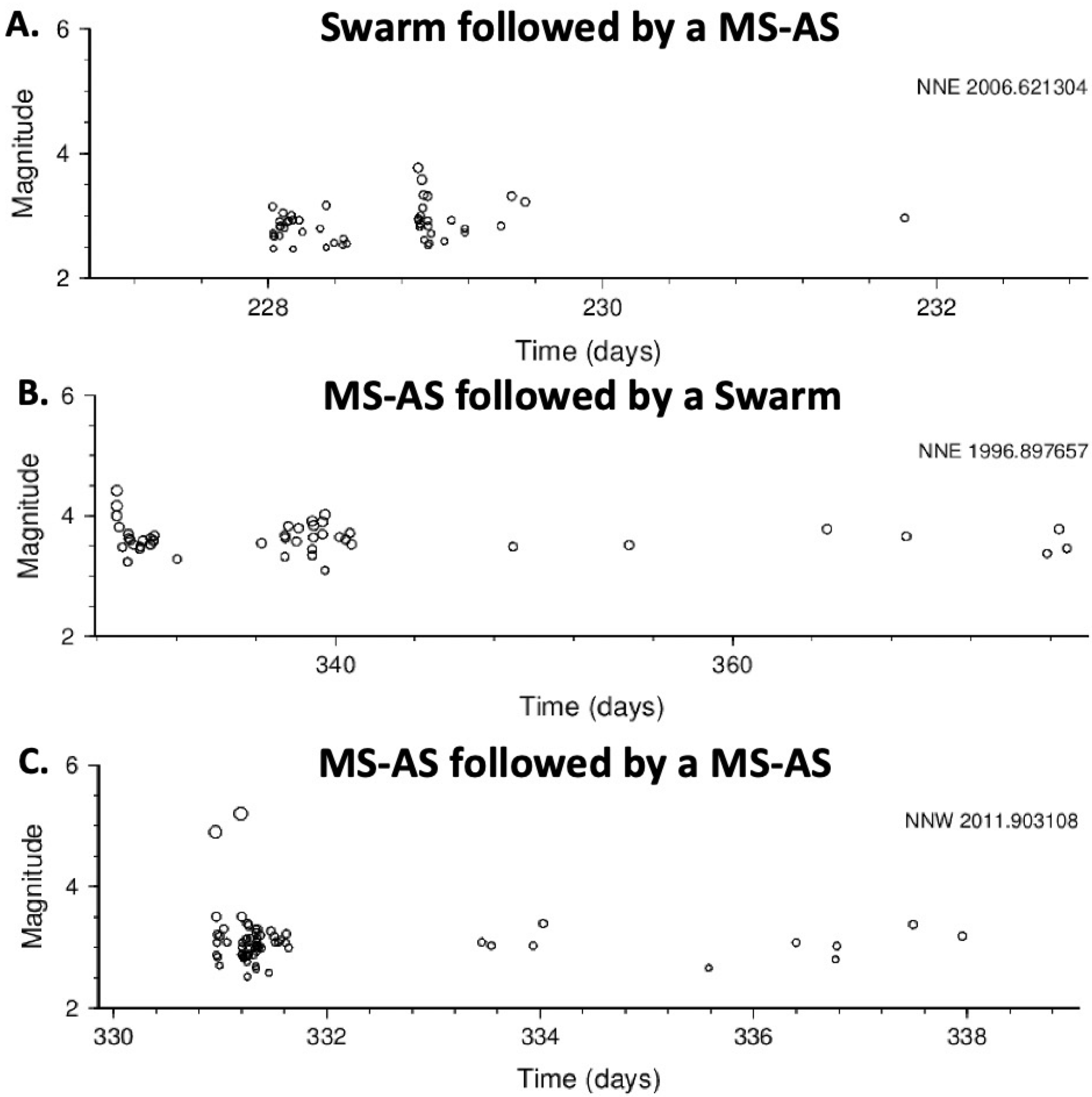

Figure 6. Examples of the additional classifications we used to describe sequences that were more complicated and had multiple characteristics.

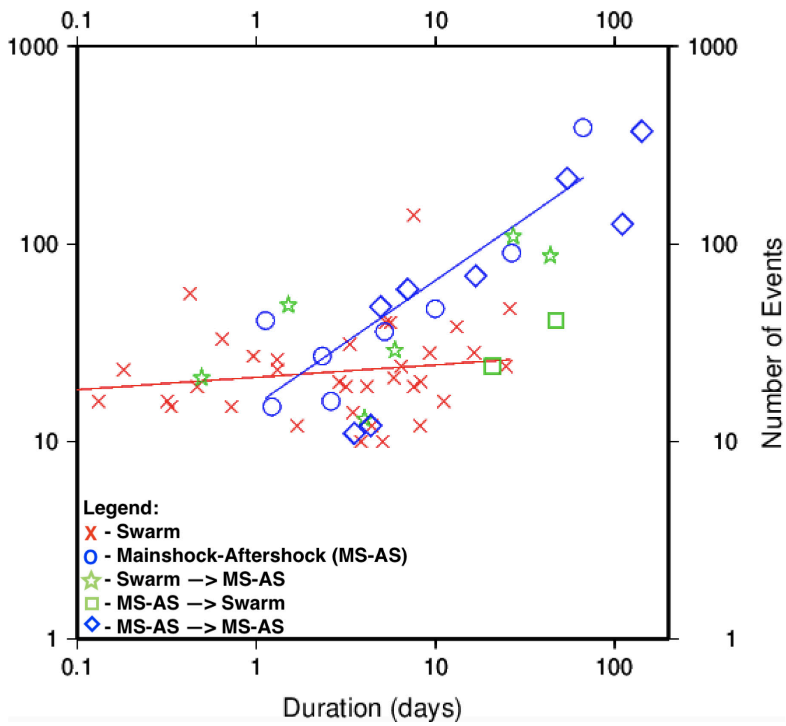

Figure 7. Duration in days of the sequence versus the number of events in the sequence. Red indicates sequences that were nominally swarms and blue indicate sequences that had predominantly MS-AS patterns. Symbol shape indicates the more detailed classification.

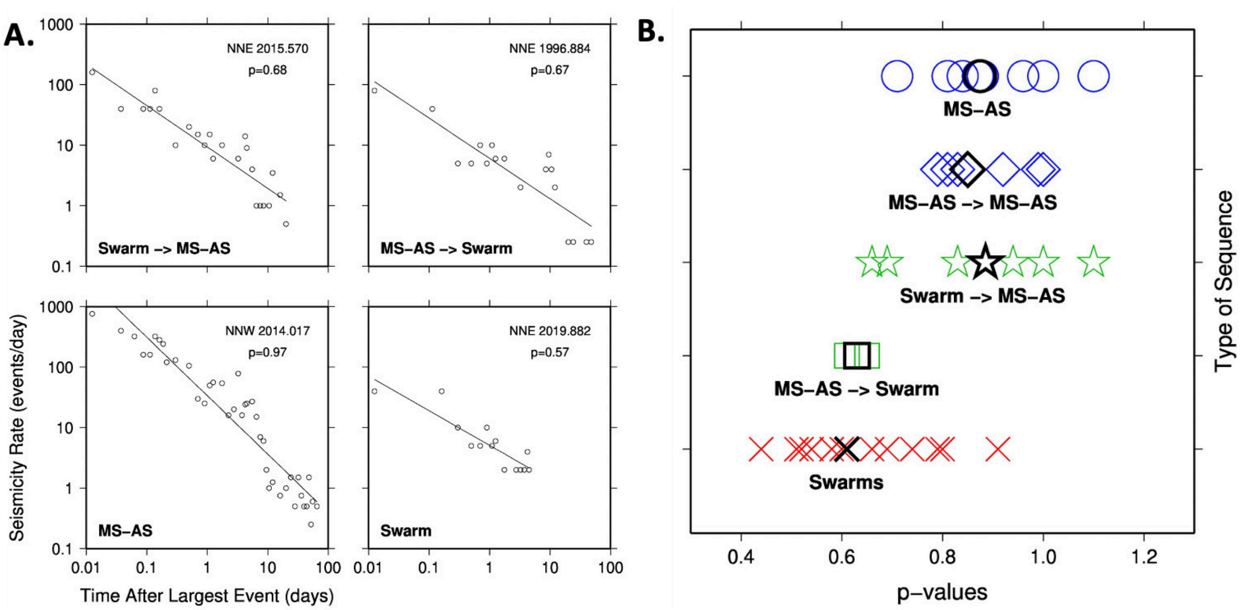

Figure 8. Estimation of the Omori p-value for sequences detected in this study. (A) Log-log plots of the seismicity rate versus the time after the largest event in the sequence for examples of 4 different sequence types. (B) Estimated p-values of the different types of sequences (colored symbols). The symbol size matches the average standard deviation of the p-value to aid in interpretation of these values.

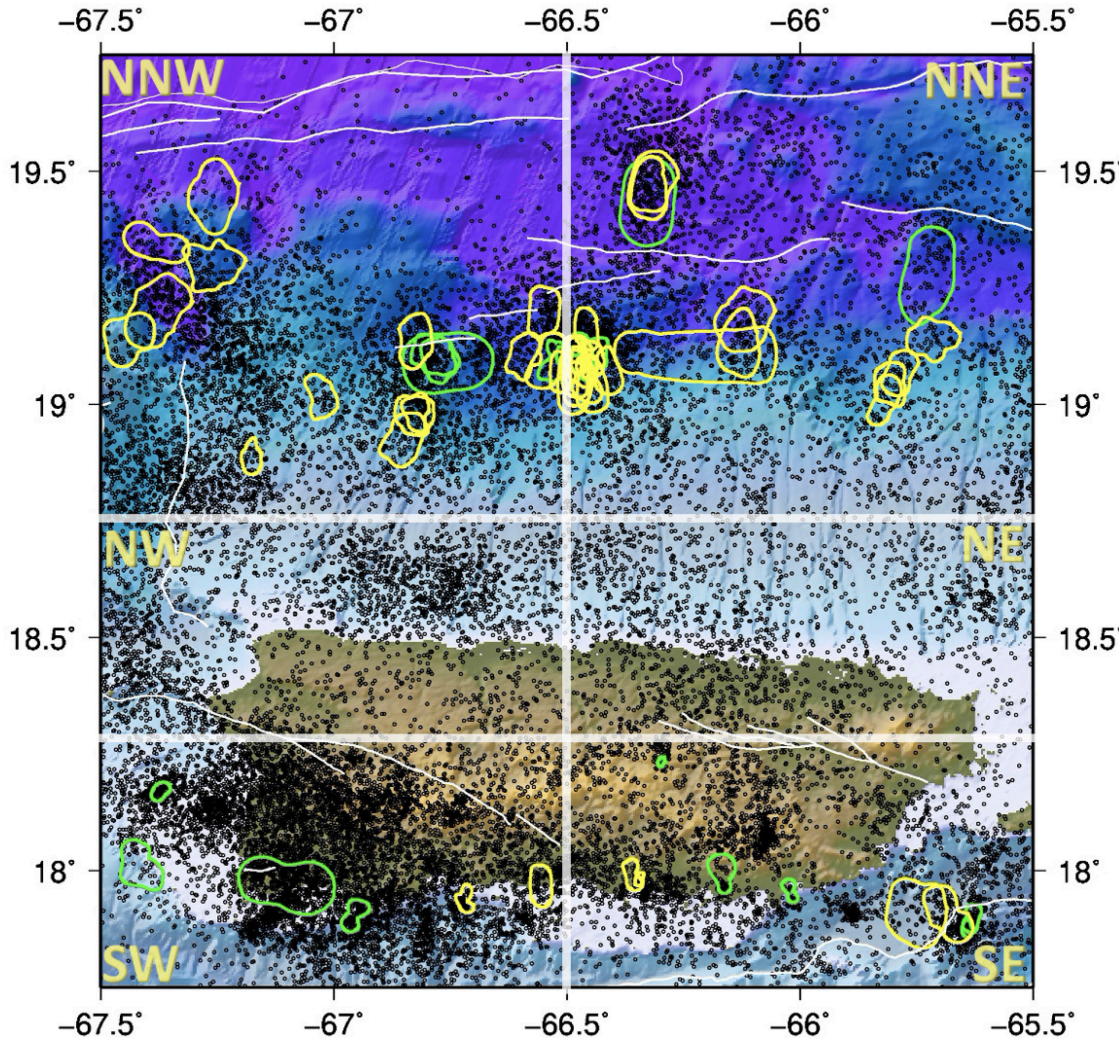

Figure 9. Map of area of study with all cataloged seismicity from PRSN in black. Thick white lines indicate the specific subdivision within the study (Figure 2). Regions outlined in green (MS-AS) or yellow (swarm) indicate the 1-sigma spatial distribution enclosing ⅔ of the events in the sequence on average. Thin white lines show mapped faults (Courtesy of E. Vanacore).